ELEMENT STRETCHING FOR A NEWTONIAN FLUID

S. BUNDITSAOVAPAK [(a)] and V. NGAMARAMVARANGGUL [(b),*]

[(a)] Department of Mathematics and Computer Science, Faculty of Science
King Mongkut's Institute of Technology Ladkrabang, Thailand

[(b)] Department of Mathematics, Faculty of Science, Chulalongkorn University

ABSTRACT

This paper presents the element-stretching problem for Newtonian fluid by finite element methods (FEM) under the semi-implicit Taylor-Galerkin pressure correction principle. The assumptions of incompressible fluid, no gravitational effect, and temperature independence are used. The two-dimensional governing equations, in which the equations are nonlinear partial differential equations, are derived through the conservation of mass and momentum.

The configuration of mesh, which is elaborately and dominantly biased, can reflect true stretching behaviour. In the paper, the variation of velocities, pressure, stresses, shear rate and extension rate have showed up to Hencky strain (ε) 1.92

The simulation programme has been created to compute the solutions, which utilize remeshing and interpolating techniques for increased accuracy of solutions. The results exhibit the same trend as the experimental solutions.

KEY WORD: Finite Element Method, Filament Stretching, Liquid Bridge

1. INTRODUCTION

Research in filament stretching is the study of fluid deformation behaviour and its properties while the fluid is stretched in time. Many people have attempted to describe and make a mathematical model since the first attempt in 1990 by Matta and Tytus [1]. It was developed by Tirtaatmadja and Sridha [2][3], who found that the behavior of filament stretching is retracted at an exponential rate. After 1996 the filament stretching research was popular, for example Spiegelberg et al. [4], Solomon and Muller [5], Sizaire and Legat [6], Yao and McKinley [7], Gaudet and McKinley [8][9], Hassagar et al. [10], Kolte and Szabo [11] and Ainser et al. [12].

Recently, M.S. Chandio et al. [13] studied numerical solution with Newtonian fluid by using semi-implicit Taylor-Galerkin/pressure-correction finite element method that was obtained by P. Townsend and M.F. Webster [14][15]. The method they used is stable and accurate up to large Henky strain levels. In contrast, K.S. Sujatha and M.F. Webster [16] simulated the filament stretching on the nano-scale under very large deformation-rates.

This paper studies the deformation of Newtonian fluid by showing the change of velocites, pressure, stresses, shear rate and extension rate of filament up to Hencky strain of 1.92. The six nodes are used in finite element method with the semi-implicit Taylor-Galerkin pressure correction scheme in two dimensionless cylindrical coordinate system. The assumptions of incompressible flow, no gravitational effect, no inertia force, and isothermal case are supposed to adopt. Tension forces at the free surface have an effect for setting both dynamic and kinematic boundary conditions. For every time-step of stretching, some techniques of remeshing, interpolation, and volume conservation are considered. In the present study, the comparison of all results have referred extensively to the fundamental work of Sizaire and Legat [6], Yao and McKinley [7], K.S. Sujatha and M.F. Webster [16] especially for M.S. Chandio et al. by constructing a C computer programme.

*Corresponding author: Tel. 662 2185220, Fax. 66 2 2552287, E-mail: vimolrat.N@chula.ac.th

2. GOVERNING EQUATIONS

For two-dimensional isothermal incompressible Newtonian fluid, the generalized momentum and continuity equations can be expressed as:

$$\rho \frac{D\vec{u}}{Dt} = \nabla \cdot \tilde{\sigma} + \rho \vec{f} \tag{1}$$

$$\nabla \cdot \vec{u} = 0 \tag{2}$$

where ρ, $\vec{u}$, t, ∇, $\tilde{\sigma}$ and $\vec{f}$ are the fluid density, the velocity vector, time, the spatial differential operator, Cauchy stress tensor and body force vector respectively. The Cauchy stress tensor is given in the form

$$\tilde{\sigma} = -p\delta + \tilde{T} \tag{3}$$

where p is an isotropic pressure and the Kronecker delta tensor is $\delta_{ij} = \begin{cases} 1, & i = j \\ 0, & i \neq j \end{cases}$

For Newtonian fluid, the extra stress tensor ($\tilde{T}$) is obtained by

$$\tilde{T} = 2\mu \tilde{D} \tag{4}$$

$$\tilde{D} = \frac{\nabla \vec{u} + \nabla \vec{u}^{t}}{2} \tag{5}$$

where $\tilde{D}$ is the rate of deformation tensor and μ is a Newtonian viscosity.

For inelastic homogeneous isotropic fluid behaviour under incompressible isothermal flow, the general form of extra stess tensor is described as a function of the rate of deformation tensor (Rivlin and Eriksen [17], Reiner[18]) that is:

$$T_{ij} = 2\mu\left(\dot{\gamma}, \dot{\varepsilon}\right) D_{ij} \tag{6}$$

where the shear rate ($\dot{\gamma}$) for simple shear flow is given by:

$$\dot{\gamma} = 2\sqrt{\mathrm{II}_d} \tag{7}$$

and elongation rate ($\dot{\varepsilon}$) for elongational flow is defined :

$$\dot{\varepsilon} = 3\frac{\mathrm{III}_d}{\mathrm{II}_d} \tag{8}$$

where II_d and III_d are the second and third invariants of the rate of deformation tensor (D_{ij}) respectively. In cylindrical coordinate system II_d and III_d are obtained by

$$\mathrm{II}_d = \frac{1}{2}\mathrm{tr}\left(D^2\right) = \frac{1}{2}\left\{\left(\frac{\partial u_r}{\partial r}\right)^2 + \left(\frac{\partial u_z}{\partial z}\right)^2 + \left(\frac{u_r}{r}\right)^2 + \frac{1}{2}\left(\frac{\partial u_r}{\partial z} + \frac{\partial u_z}{\partial r}\right)^2\right\} \tag{9}$$

and $$\mathrm{III}_d = \det\left(D\right) = \frac{V_r}{r}\left\{\frac{\partial u_r}{\partial r}\frac{\partial u_z}{\partial z} - \frac{1}{4}\left(\frac{\partial u_r}{\partial z} + \frac{\partial u_z}{\partial r}\right)^2\right\} \tag{10}$$

For convenience of comparison and representation, the problem in dimensionless form has considered. The non-dimensional variables $r^*, z^*, u^*, p^*, T^*, t^*, \mu^*, \dfrac{D}{Dt^*}, \lambda^*, \mu_i^*, \chi^*$ are the rate of dimensional variables per characteristic factor as follows:

$$r^* = \frac{r}{L},\ z^* = \frac{z}{L},\ u^* = \frac{u}{V},\ p^* = \frac{L}{\mu_0 V} p = \frac{1}{\mu_0 \dot{\varepsilon}_0} p,\ T^* = \frac{L}{\mu_0 V} T = \frac{1}{\mu_0 \dot{\varepsilon}_0} T,$$

$$t^* = \frac{V}{L} t = t \dot{\varepsilon}_0 \ ,\ \nabla^* = L \nabla \ ,\ \frac{D}{Dt^*} = \frac{L}{V}\frac{D}{Dt} = \frac{1}{\dot{\varepsilon}_0}\frac{D}{Dt} \ ,\ \lambda^* = \frac{V}{L}\lambda = \dot{\varepsilon}_0 \lambda \ ,$$

$$\mu_i^* = \frac{1}{\mu_0}\mu_i;\ \ i = 1,2,\ \dot{\gamma}^* = \frac{L}{V}\dot{\gamma} = \frac{\dot{\gamma}}{\dot{\varepsilon}_0},\ \chi^* = \frac{1}{\mu_0 \dot{\varepsilon}_0 L}\chi$$

where λ is a relaxation time, χ is a coefficient of tension, $\dot{\varepsilon}_0$ is stretching-rate, L is a characteristic length, V is a characteristic velocity ($V = \dot{\varepsilon}_0 L$), μ_0 is reference viscosity and index $i = 1,2$

3.TAYLOR-GALERKIN METHOD

The computation converts non-linear P.D.E. into the system of algebraic equations for the convenience of computation by converting expressions in terms of a time–dependent differential expression into the forward finite different form using Taylor's series expansion in time (with half time step method). For the pressure, the semi-implicit pressure correction method was used. After that, equations of pressure and velocities are separated into two by Galerkin weak formulation which includes integration by part so that the algebraic equations appear as equations (11)-(14). The way to discretise time and spatial derivatives was introduced by Donea [19].

stage 1a

$$\left(\frac{2\,\mathrm{Re}}{\Delta t}[M] + \frac{1}{2}[S_{ii}]\right)\nu_{i_k}^{n+1/2} + \frac{1}{2}[S_{ij}]\nu_{j_k}^{n+1/2} = \left(\frac{2\,\mathrm{Re}}{\Delta t}[M] - \frac{1}{2}[S_{ii}]\right)\nu_{i_k}^{n} - \frac{1}{2}[S_{ij}]\nu_{j_k}^{n}$$
$$- \mathrm{Re}\left([NR]_l\,\nu_{i_l}^{n} + [NZ]_l\,\nu_{j_l}^{n}\right) + [L_i]\,p_k^n \qquad (11)$$

stage 1b

$$\left(\frac{\mathrm{Re}}{\Delta t}[M] + \frac{1}{2}[S_{ii}]\right)\nu_{i_k}^{*} + \frac{1}{2}[S_{ij}]\nu_{j_k}^{*} = \left(\frac{\mathrm{Re}}{\Delta t}[M] - \frac{1}{2}[S_{ii}]\right)\nu_{i_k}^{n} - \frac{1}{2}[S_{ij}]\nu_{j_k}^{n} + [L_i]\,p_k^n$$
$$- \mathrm{Re}\left([NR]_l\,\nu_{i_l}^{n+1/2} + [NZ]_l\,\nu_{j_l}^{n+1/2}\right)\nu_{i_k}^{n+1/2} \qquad (12)$$

stage 2 $(\theta = 1/2)$ (Crank-Nicolson [20])

$$\theta[K]q_k^{n+1} = -\frac{\mathrm{Re}}{\Delta t}[L_i^t]\nu_{i_k}^{*}; \qquad q_k^{n+1} = p_k^{n+1} - p_k^n \qquad (13)$$

stage 3

$$\frac{\mathrm{Re}}{\Delta t}[M]\left(\nu_{i_k}^{n+1} - \nu_{i_k}^{*}\right) = \theta[L_i]q_k^{n+1} \qquad (14)$$

where $M_{ij} = \sum_k \iint_\Omega N_i N_j n_k r_k \mid J \mid d\xi d\eta$

$$(S_{rr})_{ij} = \mu \sum_k \iint_\Omega \left\{ \frac{1}{\mid J \mid} \left[2\left(J_{22}\frac{\partial N_i}{\partial \xi} - J_{12}\frac{\partial N_i}{\partial \eta} \right)\left(J_{22}\frac{\partial N_j}{\partial \xi} - J_{12}\frac{\partial N_j}{\partial \eta} \right) \right.\right.$$
$$\left.\left. + \left(-J_{21}\frac{\partial N_i}{\partial \xi} + J_{11}\frac{\partial N_i}{\partial \eta} \right)\left(-J_{21}\frac{\partial N_j}{\partial \xi} + J_{11}\frac{\partial N_j}{\partial \eta} \right) \right] \right\} n_k r_k d\xi d\eta$$
$$+ 2\mu \iint_\Omega \frac{N_i N_j}{r_1 n_1 + r_2 n_2 + r_3 n_3} \mid J \mid d\xi d\eta$$

$$(S_{rz})_{ij} = \mu \sum_k \iint_\Omega \left[\frac{1}{\mid J \mid} \left(-J_{21}\frac{\partial N_i}{\partial \xi} + J_{11}\frac{\partial N_i}{\partial \eta} \right)\left(J_{22}\frac{\partial N_j}{\partial \xi} - J_{12}\frac{\partial N_j}{\partial \eta} \right) \right] n_k r_k d\xi d\eta$$

$$(S_{zr})_{ij} = \mu \sum_k \iint_\Omega \left[\frac{1}{\mid J \mid} \left(J_{22}\frac{\partial N_i}{\partial \xi} - J_{12}\frac{\partial N_i}{\partial \eta} \right)\left(-J_{21}\frac{\partial N_j}{\partial \xi} + J_{11}\frac{\partial N_j}{\partial \eta} \right) \right] n_k r_k d\xi d\eta$$

$$(S_{zz})_{ij} = \mu \sum_k \iint_\Omega \frac{1}{\mid J \mid} \left[\left(J_{22}\frac{\partial N_i}{\partial \xi} - J_{12}\frac{\partial N_i}{\partial \eta} \right)\left(J_{22}\frac{\partial N_j}{\partial \xi} - J_{12}\frac{\partial N_j}{\partial \eta} \right) \right.$$
$$\left. + 2\left(-J_{21}\frac{\partial N_i}{\partial \xi} + J_{11}\frac{\partial N_i}{\partial \eta} \right)\left(-J_{21}\frac{\partial N_j}{\partial \xi} + J_{11}\frac{\partial N_j}{\partial \eta} \right) \right] n_k r_k d\xi d\eta$$

$$(NR)_k = \sum_\ell \iint_\Omega N_i N_k \left(J_{22}\frac{\partial N_j}{\partial \xi} - J_{12}\frac{\partial N_j}{\partial \eta} \right) n_\ell r_\ell d\xi d\eta$$

$$(NZ)_k = \sum_\ell \iint_\Omega N_i N_k \left(-J_{21}\frac{\partial N_j}{\partial \xi} + J_{11}\frac{\partial N_j}{\partial \eta} \right) n_\ell r_\ell d\xi d\eta$$

$$(L_r)_{ij} = \sum_k \iint_\Omega \left(J_{22}\frac{\partial N_j}{\partial \xi} - J_{12}\frac{\partial N_i}{\partial \eta} \right) n_j n_k r_k d\xi d\eta + \iint_\Omega N_i n_j \mid J \mid d\xi d\eta$$

$$(L_z)_{ij} = \sum_k \iint_\Omega \left(-J_{21}\frac{\partial N_i}{\partial \xi} + J_{11}\frac{\partial N_i}{\partial \eta} \right) n_j n_k r_k d\xi d\eta$$

$$\left[L_r^t\right]_{ij} = \left[L_r\right]_{ji}, \ \left[L_z^t\right]_{ij} = \left[L_z\right]_{ji}$$

$$K_{ij} = \mu \sum_k \iint_\Omega \frac{1}{|J^*|} \left[\left(J_{22}^*\frac{\partial n_i}{\partial \xi} - J_{12}^*\frac{\partial n_i}{\partial \eta} \right)\left(J_{22}^*\frac{\partial n_j}{\partial \xi} - J_{12}^*\frac{\partial n_j}{\partial \eta} \right) \right.$$
$$\left. + \left(-J_{21}^*\frac{\partial n_i}{\partial \xi} + J_{11}^*\frac{\partial n_i}{\partial \eta} \right)\left(-J_{21}^*\frac{\partial n_j}{\partial \xi} + J_{11}^*\frac{\partial n_j}{\partial \eta} \right) \right] n_k r_k d\xi d\eta$$

The solutions of all stages have been solved by Jacobi iterative method, namely successive over relaxation (SOR), with Penalty approach for handling boundary condition. The computation of integral was approximated by a triangular 4-points Gaussian quadrature approach (Reddy [21]). The Gradient recovery is a strategy to improve the stability of solution, and has been stated by Hawken et al. [22], Levine [23, 24], Boroomand and Zienkiewicz [25], Zienkiewicz and Zhu [26] and Matallah [27], who applied it to adjust the smooth convergence. At each time step, the fixed-connectivity remeshing technique is employed by adjusting values in domain with interpolation technique while the constant values of the outside part are kept. The initial estimation of free surface is computed by an elliptic equation, $h = \left(R_0 - R(t)\right)\sqrt{1 - \dfrac{z}{L(t)^2}}$ and equations (15)-(17) from the method of time dependent prediction

$$\left(\frac{\partial h}{\partial t}\right)^{n+1} = u_r^n - u_z^n \left\{\left(\frac{\partial h}{\partial z}\right)^{n-1} + \frac{1}{2}\left[\left(\frac{\partial h}{\partial z}\right)^{n} - \left(\frac{\partial h}{\partial z}\right)^{n-1}\right]\right\} \tag{15}$$

$$\left(\frac{\partial h}{\partial z}\right) = \frac{1}{\Delta z_{i+1} + \Delta z_i}\left[\frac{\Delta z_i}{\Delta z_{i+1}}\left(h_{i+1} - h_i\right) + \frac{\Delta z_{i+1}}{\Delta z_i}\left(h_i - h_{i-1}\right)\right] \tag{16}$$

$$\left(\frac{\partial^2 h}{\partial z^2}\right) = \frac{2}{\Delta z_{i+1} + \Delta z_i}\left[\frac{\left(h_{i+1} - h_i\right)}{\Delta z_{i+1}} + \frac{\left(h_i - h_{i-1}\right)}{\Delta z_i}\right] \tag{17}$$

where $\Delta z_i = z_i - z_{i-1}$

For each computational step, the conservation of volume is verified from the summation of frustum of a cone compared with the initial volume.

The convergent criteria is considered by $\left\|E(x)\right\|_\infty = \left\|\left(x^{n+1} - x^n\right)\right\|_\infty \le \mathrm{TOL}$

Here $\mathrm{TOL}=10^{-5}$ for velocity and pressure, $\mathrm{TOL}=10^{-9}$ for SOR computation, and $\mathrm{TOL}=10^{-3}$ for checking volume.

4. PROBLEM SPECIFICATION

Here, the original domain of fluid in a cylinder of height L_0 and radius R_0 are displayed as figure 1. Both end are attached to the plates and pulled in opposite directions with the same speed. At time t, the fluid is stretched in the *z*-direction with distance $L(t)$ and shrunk in the *r*-direction with distance $R(t)$ for maintaining mass conservation. According to symmetry, a quarter of the domain is considered for simulation (figure 1).

4.1 Initial condition

Initially, the computational domain is rectangular, and fluid is assumed to be at rest, i.e., velocity in both directions are zero as shown in figure 1.

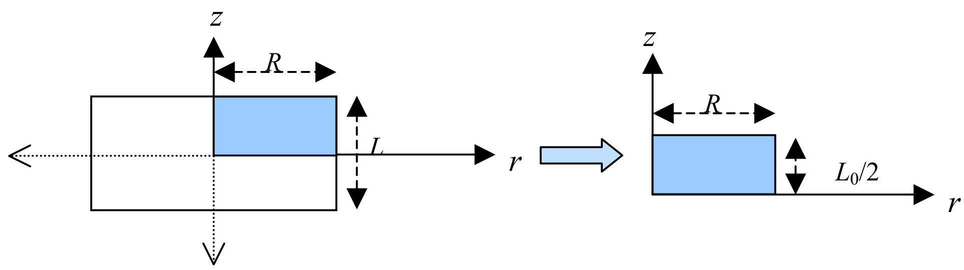

(a) (b)

Figure 1: Domain of the problem

4.2 Boundary condition

The solutions must satisfy the boundary conditions. Dirichlet boundary condition and Neumann boundary condition will be used as figure 2.

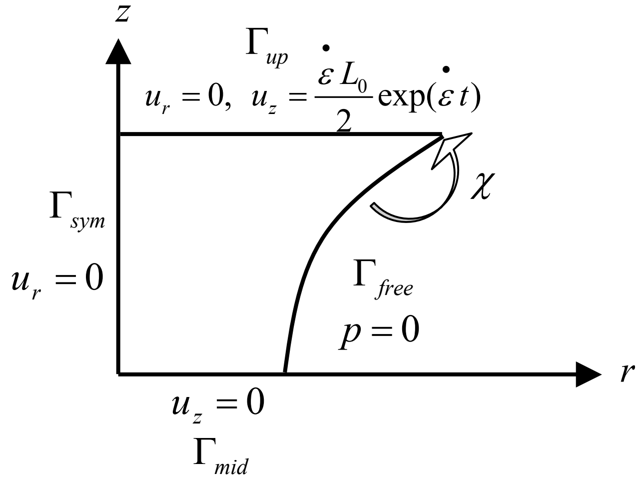

Figure 2: Boundary condition for the filament stretching

In additional, the free surface will be affected by surface tension which is defined by the following dynamic and kinematic boundary conditions:

Dynamic boundary condition

The condition comes from continuity of contact force along free surface as follow:

$$\tilde{\sigma} \cdot \hat{n} = -\left(p_{atm} + \chi\left(\frac{1}{R_1} + \frac{1}{R_2}\right)\right)\hat{n} \tag{18}$$

where $\hat{n}$ is outward normal vector, p_{atm} is atmospheric pressure, χ is surface tension coefficient, R_1 and R_2 are radius of curvature of free surface shown in figure 3 (Levich [28] and Keunings [29]) as follow:

$$R_1 = \frac{\left[1 + \left(\frac{\partial h}{\partial z}\right)^2\right]^{\frac{3}{2}}}{\frac{\partial^2 h}{\partial z^2}} \quad \text{and } R_2 = -h\left[1 + \left(\frac{\partial h}{\partial z}\right)^2\right]^{\frac{1}{2}} \tag{19}$$

where h is displacement normal to initial free surface and it is a function of time but its' value is differ for each height z as shown in figure 4.

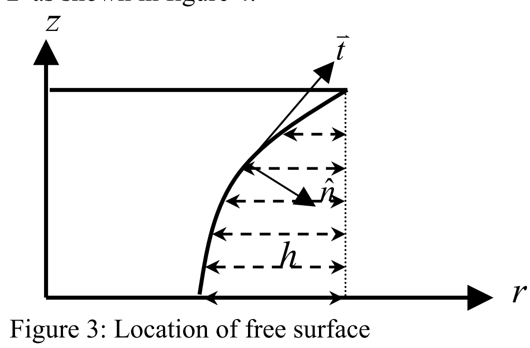

Figure 3: Location of free surface

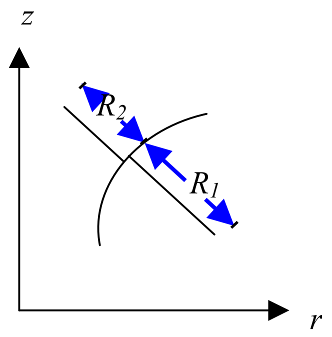

Figure 4: Radius of curvature at free surface

Kinematic boundary condition

This condition comes from the fact that free surface is material line, defined as:

$$\frac{\partial h}{\partial t} = u_r - u_z \frac{\partial h}{\partial z}; \qquad \forall t \tag{20}$$

4.3 Material parameters

When computing the Newtonian fluid case, parameters of material in Table 1 are defined on the basis of the steady shear data by McKinley [30].

Table 1. Material parameters for a polyisobuthylene-polybutene Boger fluid.

ρ (density)	890 (kg m^{-3})
$\dot{\varepsilon}$ (stretch rate)	1.6 (s^{-1})
L_0 (initial length)	2*10^{-3} (m)
R_0 (initial radius)	3.5*10^{-3} (m)
χ (surface tension coefficient)	28.9*10^{-3} (n m^{-1})
Newtonian calculation	
η (shear viscosity)	98 (Pa s^{-1})

4.4 Mesh patterns

In this problem, four patterns of meshes are shown in figure 5.

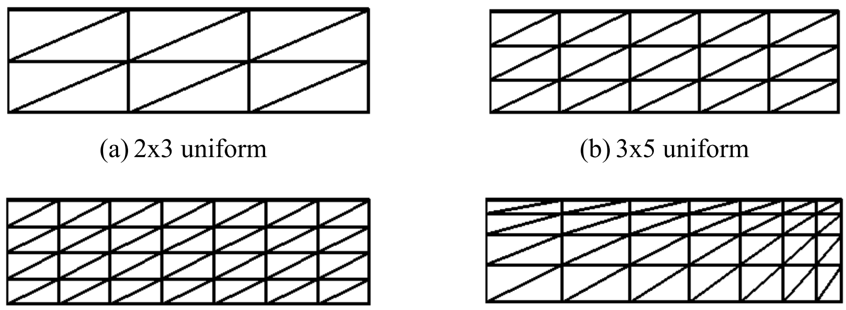

(a) 2x3 uniform (b) 3x5 uniform

(c) 4x7 uniform (d) 4x7 bias

Figure 5: Mesh patterns

5. RESULT

The configuration of the mesh, which is elaborately and dominantly biased, can reflect pure stretching behavior. Computational results of $r(z)$, $R_{\min}$ at each Hencky strain, U_r along free surface and U_z at center line are in line with the work of Chandio et al. shown in figures 6-9. The evolution of filament structure of Newtonian fluid at different Hencky strain is illustrated in figure 10.

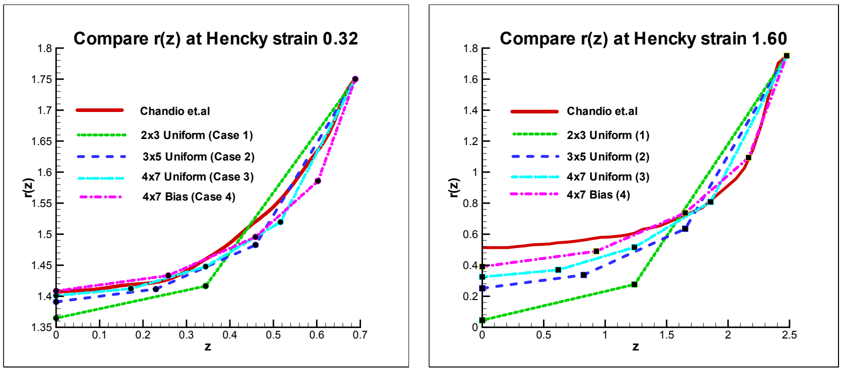

(a) $\varepsilon = 0.32$ (b) $\varepsilon = 1.60$

Figure 6: Radius $(r(z))$: comparison each mesh types with Chandio et al.

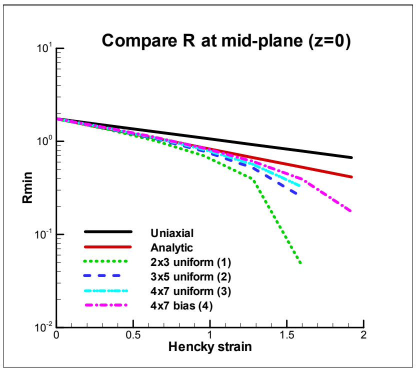

Figure 7: $R_{\min}$: comparison each mesh types with uniaxial and analytical solution

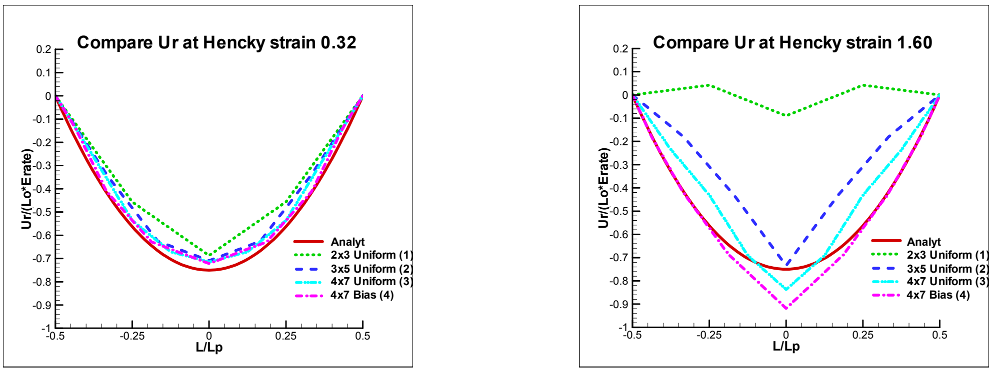

(a) $\varepsilon = 0.32$ (b) $\varepsilon = 1.60$

Figure 8: U_r profiles along free surface: comparison each mesh types with analytical solution

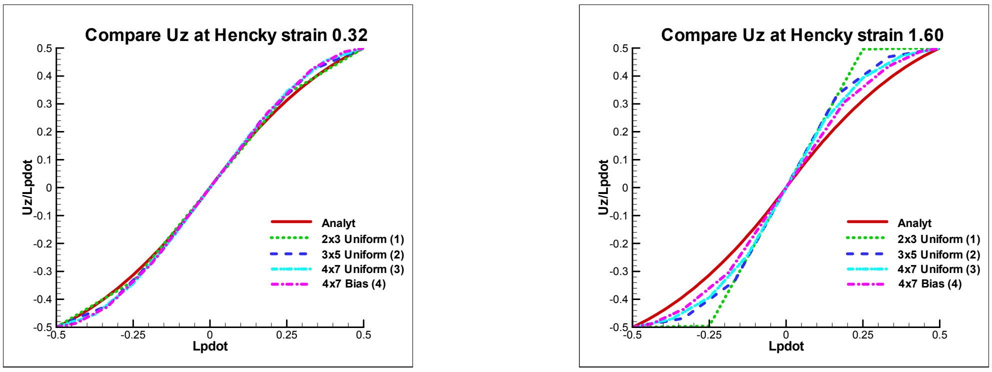

(a) $\varepsilon = 0.32$ (b) $\varepsilon = 1.60$

Figure 9: U_z profiles at centreline ($r = 0$) : comparison each mesh types with analytical solution

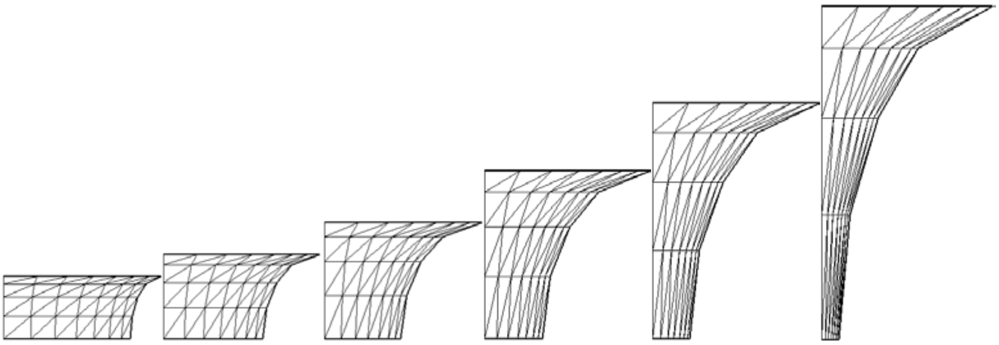

$\varepsilon = 0.32$ $\varepsilon = 0.64$ $\varepsilon = 0.96$ $\varepsilon = 1.28$ $\varepsilon = 1.60$ $\varepsilon = 1.92$

Figure 10: Evolution of filament structure of Newtonian fluid at different Hencky strain

The velocities satisfying the lubrication model of Spiegelberg et al. [4] and other research [6,7,13] is shown in each Hencky strain (ε) up to 1.92. The r direction velocity (U_r) as in figure 11 is relatively small. The greatest change at free surface of figure 12 is observed, especially at the bottom right corner, where the value is most negative. This shrinks with lower rate as Hencky strain increases, due to the reduction in fluid area, shrinking in the opposite direction to r axis. When considering the area throughout the free surface, the value U_r will satisfy lubrication model. The velocity in z direction (U_z) gives the result of figure 13, which illustrates that U_z is dependent on velocity of the plates, thus maximum at the upper plate and decreasing until it reaches 0 at the lower plate. It can also be seen that U_z changes according to the height z , and at the midplane ($r = 0$) it satisfies the lubrication model (figure 14).

The value of Pressure (P) in the initial will be changed according to distance from free surface and when ε increased, Atmospheric pressure (P_{atm}) will affect the domain more, especially at the upper-right corner shown in Figure 15.

The stress near free surface will be more smooth (more natural) when the mesh is finer, and the bias rate is greater. This comes from the gradient recovery technique. When stretching the element, the fluid near bottom plate will be stretched in z -axis and shrunk in r -axis.

This makes T_{rr} most negative and make T_{zz} most positive at this bottom plate. The effect from pulling around the circumference is very small. The effect from shearing will be cleared when ε is small and this shows that the fluid is not purely uni-axial. But when ε is increased, the effect of shearing is decreased until it is unable to be considered and becomes shear-free flow. The stress in many directions can be shown as in Figure 16-17.

Shear rate ($\dot{\gamma}$) contains component $\frac{\partial u_r}{\partial r}$ which has the greatest effect on the computational process. When undergoing Gradient recovery, it can be seen that the area near free surface $\dot{\gamma}$ does not have smooth stress, and if we stretch it to larger ε, the $\dot{\gamma}$ will increased at the bottom line. This tells us that the area is easy to deform. Shear rate is shown as in Figure 18.

Extension rate ($\dot{\varepsilon}$) is affected by the structure of mesh as for $\dot{\gamma}$, which leads to unsmooth values near the free surface area. If ε is small we can see that $\dot{\varepsilon}$ will be high according to the increasing of ε, especially at the bottom line where it reaches a maximum. This means the area is most fragile and most easy to break down (shown in figure 19).

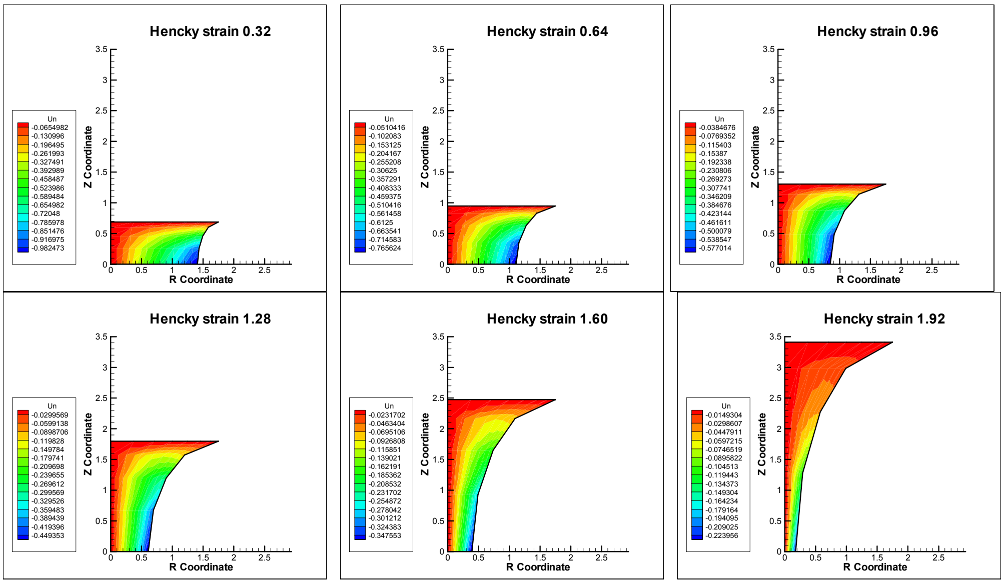

Figure 11: U_r colour contours,various Hencky strain

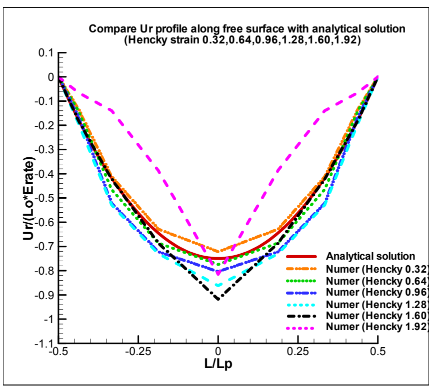

Figure 12: U_r profiles along free surface, case 4, compared with analytical solution

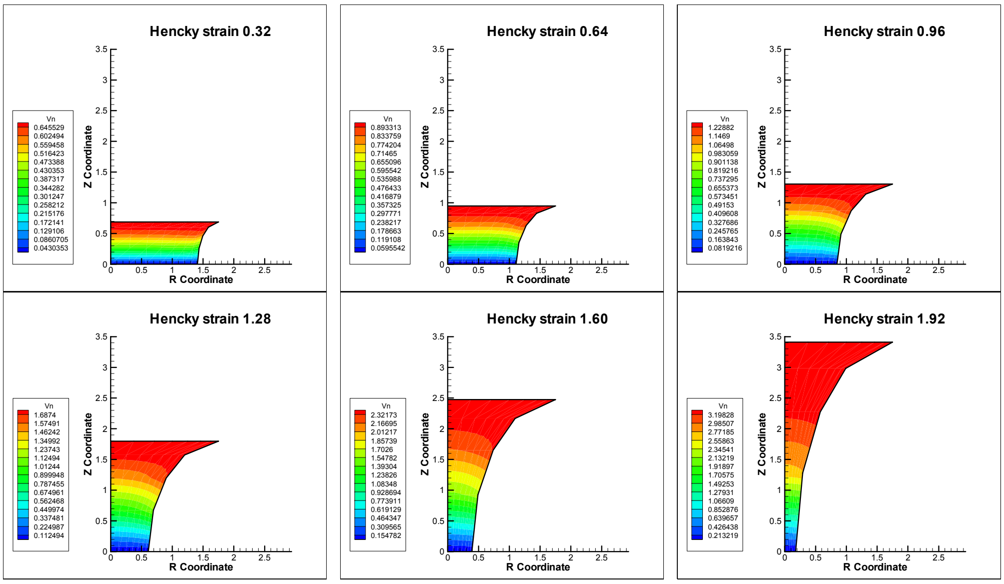

Figure 13: U_z colour contours,various Hencky strain

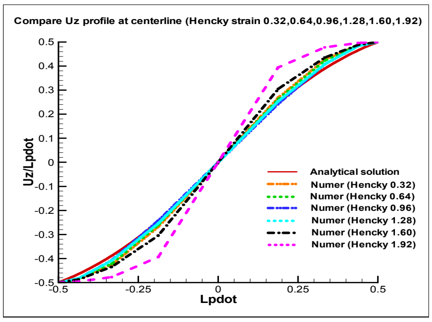

Figure 14: U_z profiles, centreline ($r = 0$), case 4, compared with analytical solution

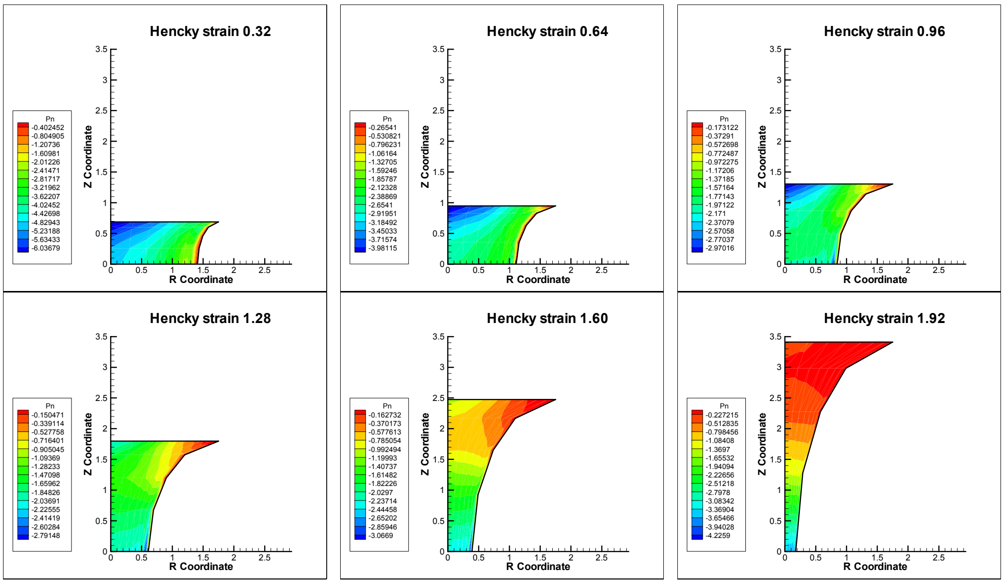

Figure 15: Pressure colour contours, various Hencky strain

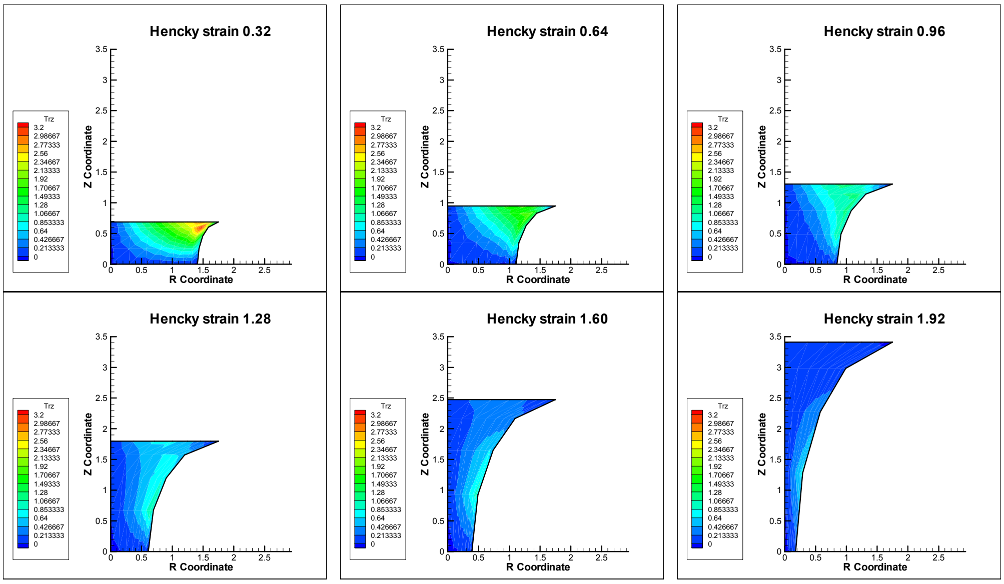

Figure 16: T_{rz} colour contours,various Hencky strain

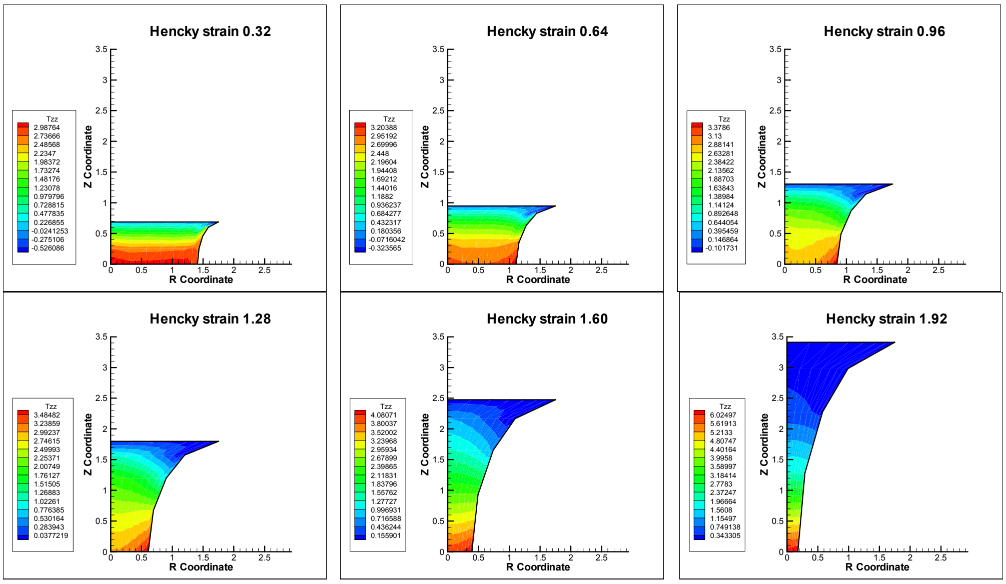

Figure 17: T_{zz} colour contours,various Hencky strain

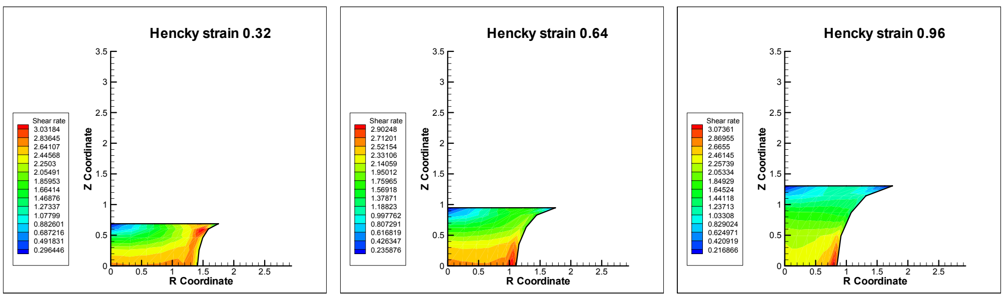

Figure 18: Shear rate colour contours,various Hencky strain

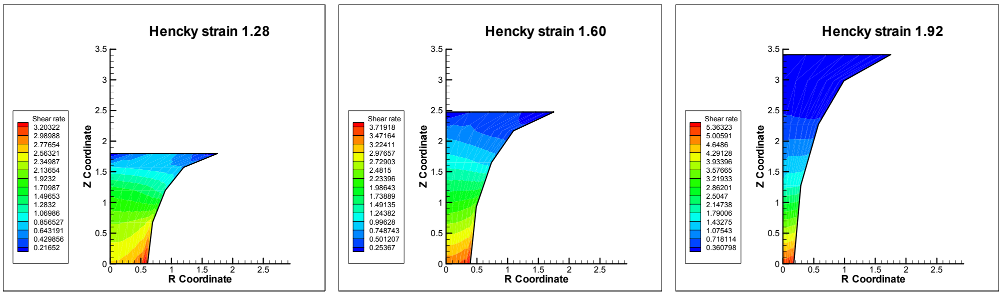

Figure 18: Continued Shear rate colour contours,various Hencky strain

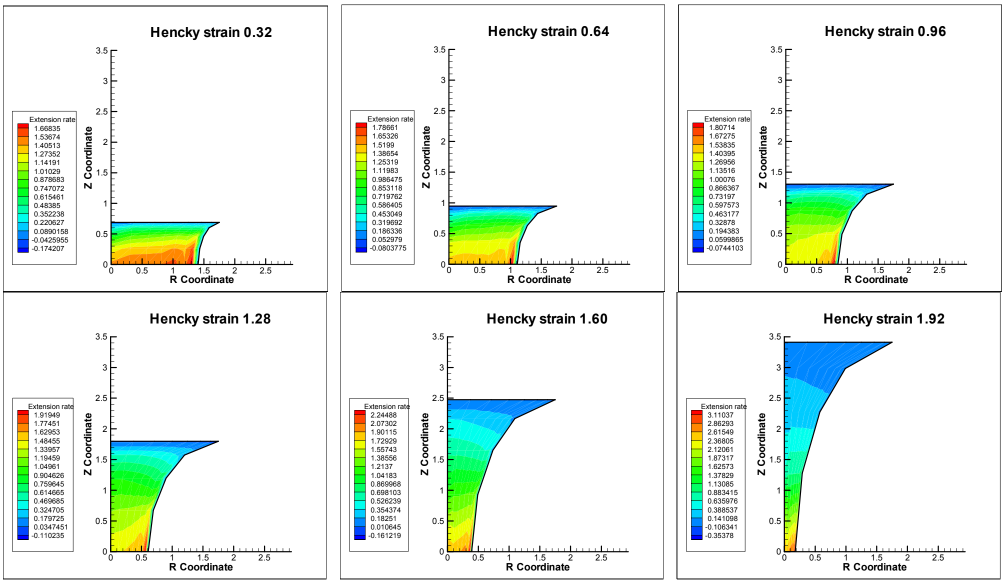

Figure 19: Extension rate colour contours,various Hencky strain

6. CONCLUSION

The structure of the mesh and initial approximation give a lot of effect to each computational step. If a configuration is chosen which is near the real situation, the computational result will be closed to the real solution.

Stretching of Newtonian fluid (with fixed viscosity) at the middle of the filament gives the most fragile and most easy to deform response.

REFERENCE:

[1] Matta J.E. and Tytus R.P., **1990**. Liquid Stretching Using a Falling Cylinder, *J. Non-Newtonian Fluid Mech*., 35, 215-229.

[2] Tirtaatmadja V. and Sridha T., **1993**. A Filament Stretching Device for Measurement of Extensional Viscosity, *J. Rheol*., 37, 1081-1102.

[3] Tirtaatmadja V. and Sridha T., **1995**. Comparison of Constitutive Equations for Polymer Solutions in Uniaxial Extension, *J. Rheol.*, 39, 1133-1160.

[4] Spiegelberg S.H., Abels D.C. and McKinley G.H., **1996**. The Role of End-effects on Measurement of Extensional Viscosity in Filament Stretching Rheometers, *J. Non-Newtonian Fluid Mech.*, 64, 229-267.

[5] Solomon M.J. and Muller S.J., **1996**. The Transient Extensional Behavior of Polystyrene-based Boger Fluids of Varying Solvent Quality and Molecular weight, *J. Rheol.*, 40, 837-856.

[6] Sizaire R. and Legat V., **1997**. Finite Element Simulation of a Filament Stretching Extensional Rheometer, *Int. J. Non-Newtonian Fluid Mech*., 77, 89-107.
[7] Yao M. and McKinley G.H., **1998**. Numerical Simulation of Extensional Deformations of Viscoelastic Liquid Bridges in Filament Stretching Device, *J. Non-Newtonian Fluid Mech*., 79, 469-501.
[8] Gaudet S. and McKinley G.H., **1996**. Extensional Deformation of Newtonian Liquid Bridges, *Phys. Fluids*., 8, 2568-2579.
[9] Gaudet S. and McKinley G.H., **1998**. Extensional Deformation of Non-Newtonian Liquid Bridges , *Comp. Mechs*., 22, 461-476.
[10] Hassager O., Kolte M.I. and Renardy M., **1998**. Failure and Non-failure of Fluid Filament in Extension, *J. Non-Newtonian Fluid Mech*., 76, 137-151.
[11] Kolte M.I. and Szabo P., **1999**. Capillary Thinning of Polymeric Filaments, *J.Rheol*., 43, 609-625.
[12] Ainser A., Carrot C., Guillet J. and Sirikov I., **2000**. *Transient Viscoelastic Analysis of Falling Weight Experiment, XIIIth Int. Cong. Rheol.* , Cambridge, UK, 2, 259-261.
[13] Chandio M.S., Matallah H. and Webster M.F., **2003**. Numerical Simulation of Viscous Filament Stretching Flows, *Int. J. Num. Meth. Heat Fluid Flow*, 13, 899-930.
[14] Townsend P. and Webster M.F., **1987**. An Algorithm for the Three-dimensional Transient Simulation of Non-Newtonian Fluid Flows, *Proc. NUMERTA 87*.
[15] Hawken D.M., Tamaddon-Jahromi H.R., Townsend P. and Webster M.F., **1990**. A Taylor-Galerkin Based Algorithm for Viscous Incompressible Flow, *Int. J. Num. Meth. Fluids*, 10, 327-351.
[16] Sujatha K.S. and Webster M.F., Transient Simulation for Nano-scale Filament Stretching with Large Deformation-rates, Research progress report, Department of Computer Science, University of Wales, Swansea.
[17] Rivlin R.S. and Eriksen J.L., **1955**. Stress Deformation Relations for Isotropic Material, *J. Rat. Mech. Anal*., 4, 323-425.
[18] Reiner M., **1960**. *Deformation Strain and Flow*, Wiley, New York.
[19] Donea J., **1984**. A Taylor-Galerkin Method for Convective Transport Problems, *Int. J. Num. Meth. Eng*., 20, 101-119.
[20] Crank J. and Nicolson P., **1947**. A Practical Method for Numerical Evaluation of Solution of Patial Differential equations of the Heat-conduction Type, *Proc. Camb. Phil. Soc*., 43, 50-67.
[21] Reddy J.N., **1984**. *An Introduction to the Finite Element Method*, McGraw-Hill.
[22] Townsend P. and Webster M.F., **1991**. A Comparison of Gradient recovery methods in Finite Element Calculations, *Comm. Appl. Num. Meth.*, 7, 195-204.
[23] Levine N., **1983**. Superconvergent Recovery of the Gradient from Finite Element Approximation on Triangles, *Technical report Num. Anal. Rep*. 6/83, University of Reading, U.K..
[24] Levine N., **1985**. Superconvergent Estimation of the Gradient from Linear Finite Element Approximation of Triangular elements, Ph.D. Thesis, University of Reading, U.K.
[25] Boroomand B. and Zienkiewicz O.C., **1997**. An Improve REP Recovery and the Effectively Robustness test, *Int. J. Num. Meth*. Eng., 40, 3247-3277.
[26] Zienkiewicz O.C. and Zhu J.Z., **1995**. Superconvergent and Superconvergent patch Recovery Finite Element in Analysis and Design, 19, 11-23.
[27] Matallah H., **1998**. Numerical Simulation of Viscoelastic Flows, PH.D. Thesis, University of Wales Swansea, U.K.
[28] Levich V.G., **1962**. Physicochemical Hydrodynamics, Prentice-Hall, Engleword Cliffs, N.J.
[29] Keunings R., **1985**. An Algorithm for the Simulation of Transient Viscoelastic Flows with Free Surface, *J. Comp. Phys.*, 62, 199-220.
[30] McKinley G.H., **1995**. Steady and Transient Motion of a Sphere Sedimenting Through Shear-thinning and Constant-vicosity Elastic Fluids, BSR Annual Award Lecture, *IX th International Workshop on Numerical Methods in Non-Newtonian Flows*.